



Universidad Autónoma
de Madrid

Biblos-e Archivo
Repositorio Institucional UAM

Repositorio Institucional de la Universidad Autónoma de Madrid

<https://repositorio.uam.es>

Esta es la **versión de autor** del artículo publicado en:
This is an **author produced version** of a paper published in:

ACS Nano 15.1 (2021): 1210-1216

DOI: <https://doi.org/10.1021/acsnano.0c08235>

Copyright: © 2021 American Chemical Society

El acceso a la versión del editor puede requerir la suscripción del recurso

Access to the published version may require subscription

Confined crack propagation in MoS₂ Monolayers by Creating Atomic Vacancies

Yolanda Manzanares Negro¹, Guillermo López-Polín^{1,2}, Kazunori Fujisawa^{3,4}, Tianyi Zhang^{4,5}, Fu Zhang^{4,5}, Ethan Kahn^{4,5}, Néstor Perea-López^{3,4}, Mauricio Terrones^{3,4,5,6,7}, Julio Gómez-Herrero^{1,8}, Cristina Gómez-Navarro^{1,8}*

¹ Departamento de Física de la Materia Condensada, Universidad Autónoma de Madrid, Madrid E-28049, Spain

² ICMN, CSIC, Madrid E 28049, Spain

³ Department of Physics, The Pennsylvania State University, University Park, PA 16802, USA

⁴ Center for 2-Dimensional and Layered Materials, The Pennsylvania State University, University Park, PA 16802, USA

⁵ Department of Materials Science and Engineering, The Pennsylvania State University, University Park, PA 16802, USA

⁶ Department of Chemistry, The Pennsylvania State University, University Park, PA 16802, USA

⁷ Institute of Carbon Science and Technology, Shinshu University, 4-17-1 Wakasato, Nagano-city 380-8553, Japan

⁸ IFIMAC Condensed Matter Physics Center (IFIMAC). Universidad Autónoma de Madrid, Madrid E-28049, Spain

Keywords: MoS₂, defects, crack propagation, toughness, Atomic Force Microscopy.

Two dimensional crystals show low resistance to fracture propagation, thus restricting their mechanical reliability. This work demonstrates controlled defect creation as an effective approach to avoid catastrophic failure in MoS₂ monolayers. A systematic study of fracture mechanics in MoS₂ monolayers as a function of the density of atomic vacancies created by ion irradiation is reported. Pristine and irradiated materials were studied by atomic force microscopy, aberration corrected high-resolution scanning transmission electron microscopy and Raman spectroscopy. By creating ruptures through nano-indentations we determine the strength and the length of propagated crack of MoS₂ atom-thick membranes containing several types of atomic vacancies. We find that while tears in pristine MoS₂ span microns length, crack propagation is strongly suppressed down to few nanometers by the presence of atomic and nanometer sized vacancies, thus increasing the material's fracture toughness.

Single-layer MoS₂ is a two-dimensional (2D) material from the family of layered transition metal dichalcogenides (TMDs), an emerging type of 2D material with appealing electronic¹ and optical properties². In particular, MoS₂ is a tunable bandgap semiconductor with potential applications in high bendable electronics³, electromechanical devices⁴ or energy storage⁵. Besides its appealing optoelectronic properties, the reliability of devices also depends on their mechanical performance, thus making mechanical failure a major concern. 2D crystals such as TMDs, present very large intrinsic strength, combined with very high fragility^{6,7}. They tend to fail in a brittle manner where catastrophic failure occurs by tearing. Therefore, preventing crack propagation in order to improve damage tolerance is essential for any application of 2D TMDs.

While much attention has been paid to the electronic properties of large area growth layers of MoS₂⁸, mechanical fracture has been little studied. Recent studies showed that fracture in high quality single layered MoS₂ is a brittle process^{9,10} in which cracks easily propagate along crystallographic directions. Cracks are usually initiated in pre-existing flaws created during growth that reduce the strength of defective areas. Theoretical calculations support that nanoscale defects could become a significant strength-limiting factor^{11,12}. Interestingly, they also predict that simultaneously they will restrain crack propagation¹³.

In this communication we provide a systematic study of the fracture properties of MoS₂ monolayers as a function of the density of different types of atomic vacancies. In particular, two types of defects were created in suspended MoS₂ monolayers; single atomic vacancies created by Ar⁺ irradiation and larger multi-atomic vacancies generated via Ga⁺ bombardment. We then performed nano-indentation experiments on these monolayers prepared with consecutive irradiation doses. Our results show that, for the same average distance between defects, the

breaking strength of MoS₂ monolayers is reduced to a factor of two by the introduction of low densities (<0.2%) of atomic vacancies while the effect of nanometer-sized vacancies yielded a fivefold decrease in strength. Scanning electron microscopy (SEM) images of the damaged membranes after indentation showed that the presence of atomic scale defects reduces tear propagation from several microns to few nanometers. Fracture toughness monotonously increased as the mean distance between the generated vacancies decreased.

Our experiments were performed on MoS₂ monolayered drumheads of 0.5-2 microns in diameter (see **Figure 1a** and b). Our starting MoS₂ monolayers were grown by CVD and then transferred by an all dry technique¹⁴ onto SiO₂/Si substrates with predefined micrometric circular wells yielding suspended membranes of MoS₂ well anchored on the circular perimeter as reported previously^{7,14,15}. The presence of single layer MoS₂ was identified by fluorescence microscopy¹⁶ and then imaged by Atomic Force Microscopy (AFM), in non-contact dynamic mode, to avoid damaging the samples (see SI1 for sample preparation and initial characterization). Only single layer drumheads exhibiting no observable slack or wrinkling (as exemplified in Figure 1b) were selected for this study.

Nanoindentations were performed at the center of the circular suspended monolayer using the tip of an AFM with a loading rate of 150 nm/s until fracture (see figure 1c and SI2 for further experimental details). Our force (F) vs. indentation (δ) curves showed a cubic dependence, thus fitting the expression¹⁷:

$$F(\delta) = \pi T \delta + \frac{E}{a^2} \delta^3 \quad \text{equation 1}$$

where T is the pre-tension accumulated in the sheet, E is the two-dimensional elastic modulus of the membrane, and a is its radius (see SI4 for more details on $F(\delta)$ curves and elastic properties).

The fracture point was experimentally determined in the indentation curves as a marked discontinuity in the applied force exemplified in Figure 1d. Under these indentation conditions, the maximum strain of the suspended MoS₂ is achieved in the region in contact with the AFM tip apex ($\bar{\rho}_c$, several nm in radius), while the rest of the monolayer remains much less strained¹⁸ (under 1%). It is therefore under the tip where the initial fracture takes place. The breaking strength (σ) at this point can be estimated using the following approximation¹⁸

$$\sigma = (F_{\text{break}} E / 4\pi R_{\text{tip}})^{1/2} \quad \text{equation 2}$$

where R_{tip} is the radius of the AFM tip. While detailed studies have shown that this expression slightly overestimates the strength⁶, it has been widely used in the literature⁷. Our indentation curves on as-prepared samples yielded values of $E = 200 \pm 20 \text{ N/m}$ for the two dimensional elastic modulus and $\sigma = 10.2 \pm 1 \text{ N/m}$ for the breaking strain, in agreement with previous reports^{7,14}.

After the initial characterization of as-grown layers, two types of defects were created in our samples. To this end, different samples were irradiated in high-vacuum under different conditions and subsequently characterized by high-resolution scanning transmission electron microscopy (HR-STEM). A batch of samples was irradiated with Ar⁺ ions at 500 eV with different irradiation doses. The doses were estimated by *in-situ* measuring the ionic current in the sample during Ar⁺ irradiation. Representative HR-STEM images of these samples are shown in **Figure 2** and SI3. Statistics performed on more than 10 similar images revealed that irradiation under these conditions generated mainly sulfur mono-vacancies (~80% of created defects) and a smaller percentage of single Mo vacancies and double sulfur vacancies, as illustrated in the lower images of figure 2. Consecutive doses yielded lower mean distances between defects ($\langle l_D \rangle$). A second batch of samples was irradiated with gallium ions (Ga⁺) using a focused ion beam. HR-STEM imaging of these samples exhibited large multi atomic vacancies; at low ion

dose most of the defects were vacancies of few-molybdenum atoms with several sulfur atoms surrounding ($V_{x\text{Mo}+y\text{S}}$). With increasing the ion dose, the atomic vacancies merge and form *nm*-sized holes.

HR-STEM imaging is a highly accurate technique to determine the concentration and type of defects. However, it is also time consuming and requires expertise to avoid damaging the samples during imaging. We also performed a detailed Raman spectroscopy study on the irradiated samples. By comparing HR-STEM and Raman spectra, we established closed relations between Raman peak intensities and frequency shifts with defect density. Thus, we could avoid HR-STEM imaging for the samples used for this study. It is well known that Raman spectrum of pristine MoS_2 presents two prominent peaks¹⁶, E' (382cm^{-1}) and A' (407cm^{-1}) associated with in-plane and out-of-plane vibrations. Due to changes in the restoring force of the atomic bonds the distance between these peaks increases when sulfur vacancies are introduced¹⁹. The addition of disorder also gives rise to a new Raman peak, LA (227 cm^{-1})²⁰. Figure 3a depicts representative spectra of an as-grown (black curve) and a Ga^+ irradiated sample (red curve). The spectra illustrate the above-mentioned peak structure and evidences the evolution from pristine to defective. By combining Raman spectra obtained at different irradiation doses and HR-STEM images we built two different plots for Ar^+ irradiated samples: Figure 3b portrays the dependence of the Intensity ratio $-I(\text{LA})/I(E')$ (black) and $I(\text{LA})/I(A_1')$ (red)- vs. mean defect distance. These intensity ratios and defect distances are related as $\frac{I(\text{LA})}{I(X)} = \frac{C(X)}{\langle l_D \rangle^2}$ where $C(X)$ is a constant that can vary with the laser energy and X can be either E' or A' peak²⁰. From our plots we obtained $C(E')=0.235$ and $C(A')=0.125$ for a laser wavelength of 532 nm. The frequency shift ($A_1' - E'$) also grows with defect concentration, but saturates for high concentrations (figure 3c). We also performed Raman spectroscopy combined with HR-STEM for gallium irradiated monolayers. We describe further details and additional information on Raman spectra in SI3.

The irradiated samples were then indented until achieving the failure point under the same conditions as the as-grown samples. **Figure 4a** displays three representative $F(\delta)$ curves for pristine and defective monolayers where the breaking load is marked with a circle. Fitting indentation curves to equation 1 yielded the values of the elastic modulus and pretension of Ar^+ irradiated drumheads revealing an average trend where the elastic modulus decreases with irradiation dose from $E_{2D}=200$ N/m for non-irradiated samples to $E_{2D}=170$ N/m for the higher irradiation dose (see SI4 for elastic characterization). Interestingly, Ga irradiated membranes showed a greater decrease of the elastic modulus. However, evaluation of the highest Ga irradiated samples wasn't feasible through this procedure since their fracture took place at forces too low for reliable fitting of the data.

The plot in panel 4b depicts the two-dimensional breaking strain (σ) as a function of the mean distance between created defects. As appreciated, the introduction of a density of defects below 0.2% significantly reduces the breaking strain. The effect of multi vacancies (in Ga irradiated samples) is much more pronounced than that of atomic vacancies; i.e for a mean defect distance of ~ 13 nm, the presence of multi-vacancies reduces the strength in a factor of ~ 2 , while for atomic vacancies the reduction does not reach a factor of 0.8.

A quick and rough estimation of toughness can be done according to the Griffith expression, $C=\sigma(b)^{1/2}$ where σ is the breaking strength and b is the largest in-plane vacancy length found in each sample. Results are portrayed in table 4c. This estimation is also suited to investigate the applicability of the Griffith criterion at the atomic scale. Griffith criterion is one of the most used thermodynamic rules describing fracture of defective materials²¹. As most mechanical theories used in engineering, this rule was developed for large structures and its validity in nanoscale systems is still uncertain²². From our measurements we obtain a nearly constant value of C for all samples, except for the pristine case (as-grown), where the value is significantly

larger than the rest. This might be due to a stronger overestimation of σ using expression 2 for the as-grown case or to a brittle to ductile transition in the presence of atomic vacancies as suggested in other studies¹⁰ (it is well accepted that this simple expression is only valid for purely brittle fracture and underestimates toughness in ductile materials). Nevertheless, from these data we deduce that the size of the vacancies has a deeper influence in the strength of the monolayers than the density of vacancies, which is in good agreement with the Griffith criterion and suggests that this century-old thermodynamic rule is still practical at the atomic scale.

With the aim of measuring crack propagation, drumheads were imaged by SEM after their failure at indentation experiments. **Figure 5** displays four representative SEM images of several membranes with increasing density of defects from left (pristine) to right (highest density of defects). As evident from this sequence of images, as-grown monolayers showed large (microns length) tears with straight and sharp edges as expected for brittle fracture and crack propagation along crystallographic directions. In contrast, the maximum edge lengths exposed after indentations in irradiated membranes, are significantly smaller reaching few nanometers in length and exhibiting a clear dependence with defect density, as observed in Figure 5e. For Ga irradiated membranes the tearing length was limited to the notch created by the section of the tip embedded in the MoS₂ monolayer during the fracture process (see SI5); for these monolayers we can only provide an upper bound for crack length.

Further quantitative information of the fracture toughness can be extracted from the stress intensity ratio. In our geometrical set up the strain in the membrane is mainly accumulated under the tip apex and the rest of the membrane remains under a very moderate strain¹⁸ that relaxes as soon as the crack is initiated¹⁰. Therefore, crack propagation is mainly governed by residuals strains in the membrane (as observed previously in similar experiments for graphene²³) and the

appropriate expression for estimating the K_C is that derived by Bhat^{24,25} for indentation geometry (further discussion in SI5).

$$K_{IC} = 1.6 E^{0.4} P^{0.6} \rho^{-0.7} \left(\frac{c}{\rho} \right)^{-0.36}$$

where E is the three-dimensional elastic modulus, P is the loading force applied at the rupture (in grams), ρ is the indenter radius (AFM tip) and c is the radius of the imaged crack. The stress intensity factor is plotted as a function of the mean distance between defects in Figure 5e. As observed, the inclusion of atomic scale vacancies yields an enhanced toughness of the MoS₂ monolayers.

Our findings can be qualitatively understood in the frame of several theoretical works^{13,26} where molecular dynamics simulations show that crack propagation in MoS₂ monolayers is governed by sulfur vacancy concentration ahead of the crack tip; while in pristine MoS₂ crack propagates through a preferential direction with least energy release, sparse vacancies create crack deflection and therefore strain energy. Furthermore, sulfur vacancies and weakly bonded sulfur atoms coalesce to form line defects, thus helping the crack tip to sustain very high, localized stress level¹³. Indeed our K_C values and observed tendencies are in striking agreement with those calculated by molecular dynamic simulations in ref¹³.

Previous experimental studies have reported crack dynamics in MoS₂ monolayers under atomically resolved HR-STEM imaging. It is accepted that in these experiments the results are influenced by the electron irradiation at high energies required for imaging; the crack usually starts at nanometer-sized holes created by the electron beam^{10,13} and fracture propagation is governed by knock-on damage during electron irradiation¹³. In contrast, in this study, the crack starts growing at atomic vacancies similar to those found in as-grown samples and crack

propagation takes place in ambient conditions, thus making our results expandable to usual application environments.

In previous works, the authors discussed their results in terms of dislocation nucleation near the crack tip ¹⁰ and suggested defect or dopant creation as a manner to control fracture dynamics. Here we go one step forward and provide a systematic study showing that defect engineering can indeed tune fracture properties by preventing crack propagation and delaying mechanical failure.

FIGURE 1

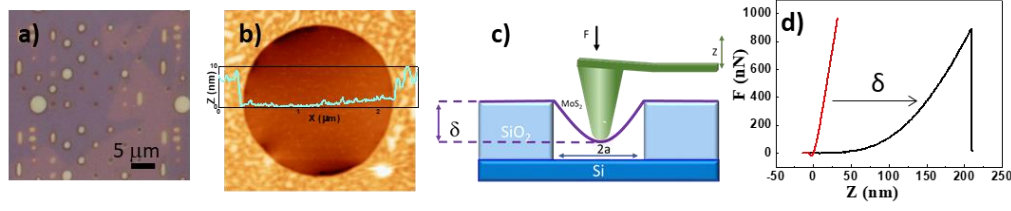


Figure 1: Experimental set up and sample. a) Optical image of a representative sample of MoS₂ monolayer on SiO₂ (300nm)/Si substrates, where the MoS₂ layer covers several pre-defined circular wells. b) AFM topography image of a MoS₂ drumhead. Inset is a profile on the central line of the image. c) Scheme of the experimental setup used for indentations. d) Representative Force vs. sample displacement (Z) curves acquired on a hard substrate (red) and a MoS₂ membrane (black). Indentation is defined as the difference between these magnitudes for a given force.

FIGURE 2

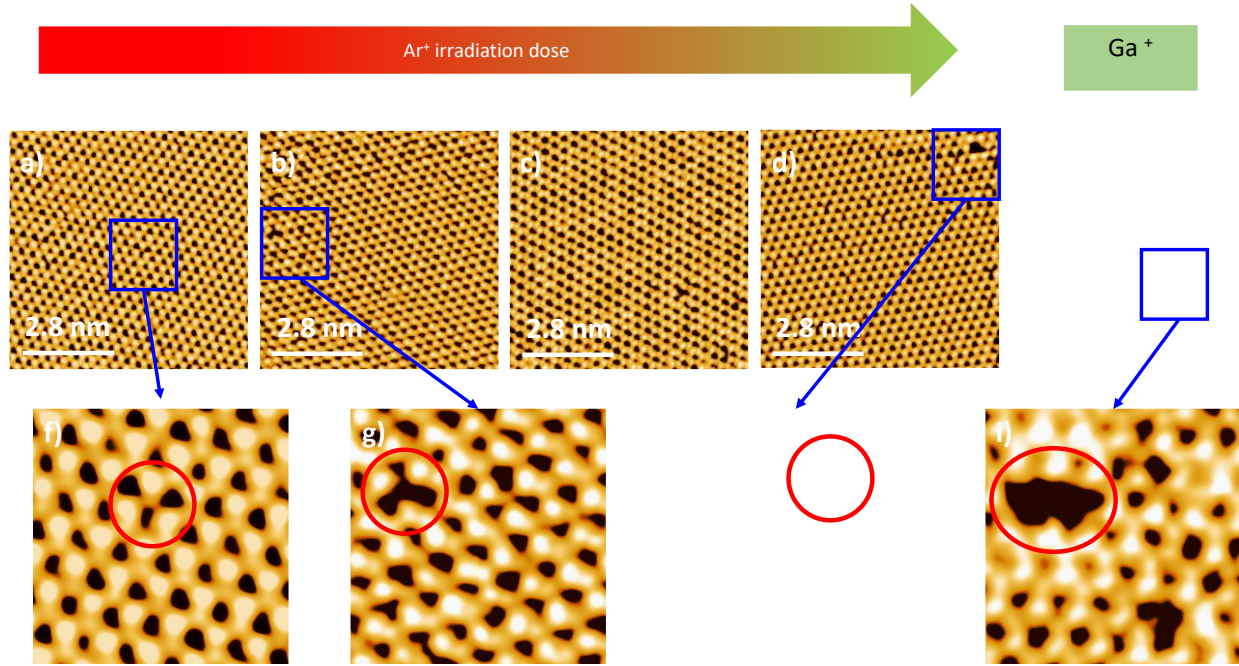


Figure 2: HR-STEM images of irradiated MoS₂ monolayers.

a) HR-STEM image of a pristine MoS₂ sample. As grown samples showed very low density of defects. These were mainly sulphur vacancies. b) c) d) representative HR-STEM images of three MoS₂ samples irradiated with 3,4 7,1 18.5 x10¹² Ar ions/cm² respectively. e) STEM image of a Ga irradiated sample (25 x10¹² ions/cm²). f) zoom-in on panel a showing a single sulphur vacancy. g) zoom on panel b showing a double sulphur vacancy h) zoom on panel c showing a Mo vacancy. These vacancies are usually accompanied by sulphur vacancies and distortions of the atomic lattice, as exemplified here. i) zoom on panel e showing a multi-atomic nanometric vacancy. We observe that single sulphur vacancies are numerous and present in all images. In order to enhance the vacancies we applied a low pass frequency filter based on Fourier's analysis to the raw images.

FIGURE 3

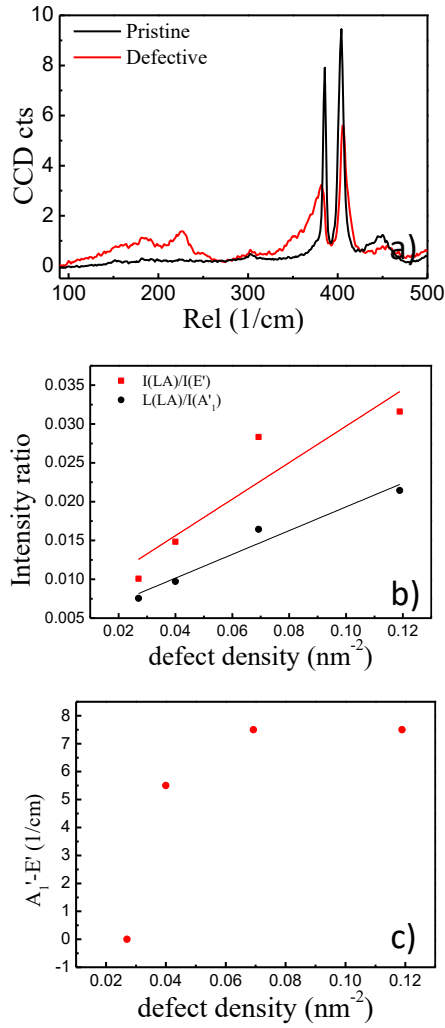


FIGURE 3. Raman-HR-STEM relationships of irradiated MoS₂ membranes. a) Raman spectra of a MoS₂ pristine (black) and irradiated (red) samples. The higher the concentration of defects the lower and wider the peaks. b) Intensity ratio for $I(LA)/I(E')$ (black) and for $I(LA)/I(A_1')$ (red) vs. mean defect distance. Both ratios exhibit a clear increase with defect concentration. c) Frequency shift ($A_1' - E'$) vs. mean defect distance. In this case the shift tends to saturate with defect concentration.

FIGURE 4

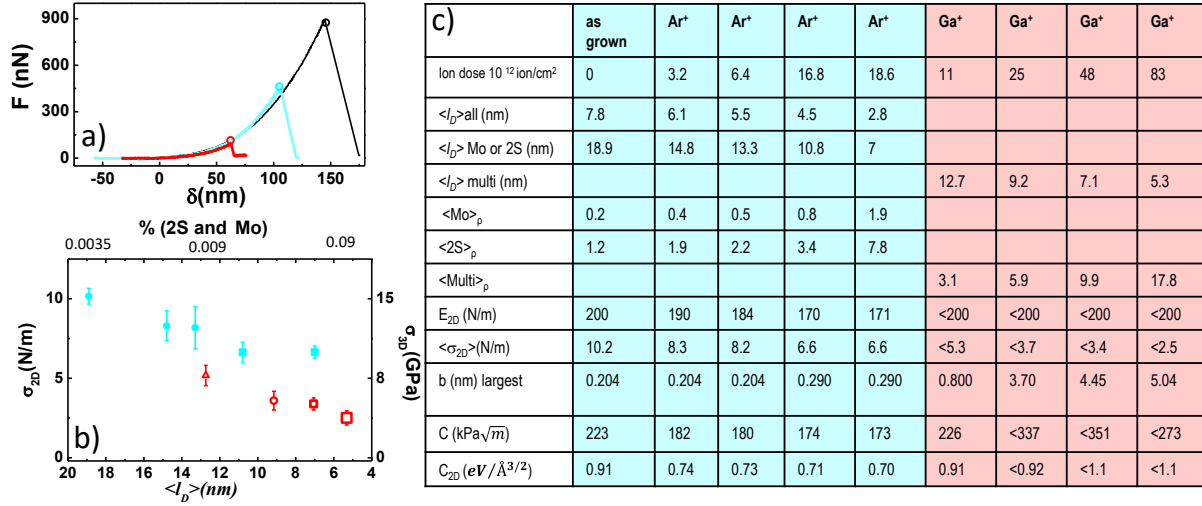


Figure 4. a) Three representative $F(\delta)$ curves for as prepared (black), Ar^+ irradiated (cyan) and Ga^+ irradiated (red) MoS_2 membranes. b) Breaking strain measured for Ar^+ (cyan) and Ga^+ (red) irradiated samples. The breaking strength was calculated according to eq. 2 in the main text. Horizontal axis corresponds to the mean distance between the largest vacancies present in each type of sample. For the case of Ar^+ irradiation both Mo single vacancies and double sulfur vacancies (2S) were considered. For the case of Ga^+ bombarded samples we only considered multi atomic vacancies.

c) Table summarizing measured and estimated values:

Ion dose: ion density received by the samples during irradiation.

<I_D>all: mean distance between any defect present in the sample (S vacancies, Mo vacancies, 2S vacancies).

<I_D> Mo or 2S: Mean distance between defects, only considering Mo vacancies and double sulfur vacancies.

<I_D> multi: Mean distance between large multivacancies.

<Mo>_ρ: Mean number of Mo vacancies in the tip-membrane contact region (ρ).

The tip-membrane contact region (ρ) was estimated as

$$\rho = \sqrt{\frac{3}{2\pi} \left(\frac{F}{EhR} + 6\pi\epsilon_0^2 \right) - 3\epsilon_0 R}$$

where R is the tip radius, F the loading Force, E the elastic modulus of the layer, h its thickness and ϵ_0 the prestress.

<2S>_ρ: mean number of double sulfur vacancies in the tip-membrane contact region.

<multi>_ρ: mean number of multi-vacancies in the tip-membrane contact region.

E_{2D}: calculated from the measured $F(\delta)$ curves according to SI4.

<σ_{2D}>(N/m): breaking strength calculated according to expression 2 in the main text.

b (nm) largest: largest length of the vacancies present in the sample.

We have taken 0.204 nm for double sulfur vacancies and 0.290 for the Mo vacancy.

C (MPa√m): C was calculated as $C = \sigma\sqrt{b_{largest}}$. For columns 1-3 we have used b=0.204 nm for the 2S vacancies, while for columns 4-5 we have utilized b=0.290 nm since the mean number of Mo vacancies in the contact area is higher than 0.8/1.

C_{2D} (eV/Å^{3/2}).

FIGURE 5

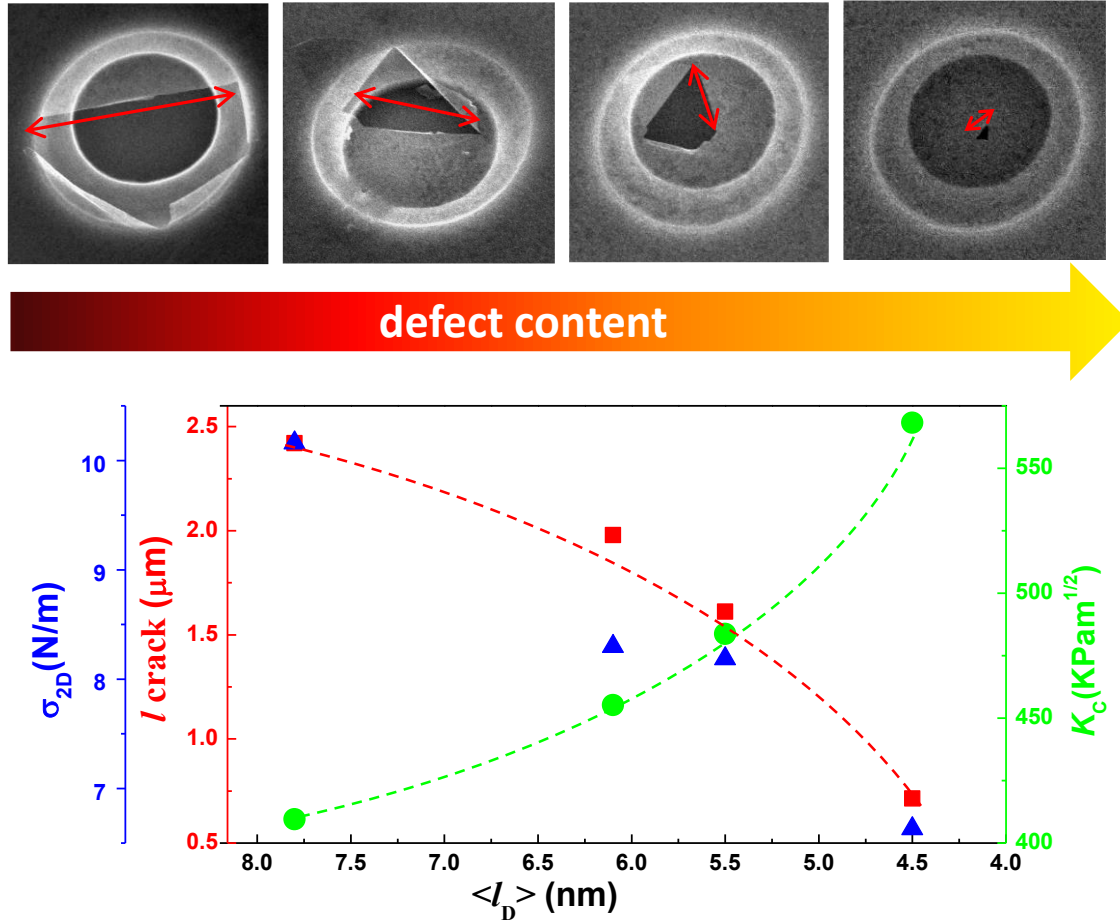


Figure 5. Panels a) to d) show representative SEM images of MoS₂ drumheads after rupture irradiated with increasing Ar⁺ doses of 0, 3.2; 6.4; 16.8 x 10¹² ion/cm² respectively. e) The graph depicts: BLUE: strength (σ_{2D}), RED, maximum crack length measured for each irradiation dose, and GREEN: toughness, stress intensity factor, as a function of the mean distance between defects created by controlled irradiation. Dotted lines are just a guide to the eye

ASSOCIATED CONTENT

Supporting Information.

The following files are available free of charge.

Supporting Information (PDF)

AUTHOR INFORMATION

Corresponding Author

Cristina Gomez-Navarro email: cristina.gomez@uam.es

Author Contributions

The manuscript was written through contributions of all authors. All authors have given approval to the final version of the manuscript.

Funding Sources

Financial support is acknowledged from MAT2016-77608-C3-3-P, S2018/NMT-451, FLAG-ERA JTC2017 and Ramon Areces foundation.

REFERENCES

- (1) Lee, C.-H.; Lee, G.-H.; van der Zande, A. M.; Chen, W.; Li, Y.; Han, M.; Cui, X.; Arefe, G.; Nuckolls, C.; Heinz, T. F.; Guo, J.; Hone, J.; Kim, P. Atomically Thin p–n Junctions with van Der Waals Heterointerfaces. *Nat. Nanotechnol.* **2014**, *9* (9), 676–681. <https://doi.org/10.1038/nnano.2014.150>.
- (2) Voshell, A.; Terrones, M.; Rana, M. Review of Optical Properties of Two-Dimensional Transition Metal Dichalcogenides. In *Wide Bandgap Power and Energy Devices and Applications III*; International Society for Optics and Photonics, 2018; Vol. 10754, p 107540L. <https://doi.org/10.1117/12.2323132>.
- (3) Akinwande, D.; Petrone, N.; Hone, J. Two-Dimensional Flexible Nanoelectronics. *Nat. Commun.* **2014**, *5* (1), 1–12. <https://doi.org/10.1038/ncomms6678>.

- (4) Manzeli, S.; Dumcenco, D.; Migliato Marega, G.; Kis, A. Self-Sensing, Tunable Monolayer MoS₂ Nanoelectromechanical Resonators. *Nat. Commun.* **2019**, *10* (1), 4831. <https://doi.org/10.1038/s41467-019-12795-1>.
- (5) Chhowalla, M.; Shin, H. S.; Eda, G.; Li, L.-J.; Loh, K. P.; Zhang, H. The Chemistry of Two-Dimensional Layered Transition Metal Dichalcogenide Nanosheets. *Nat. Chem.* **2013**, *5* (4), 263–275. <https://doi.org/10.1038/nchem.1589>.
- (6) Lee, C.; Wei, X.; Kysar, J. W.; Hone, J. Measurement of the Elastic Properties and Intrinsic Strength of Monolayer Graphene. *Science* **2008**, *321* (5887), 385–388. <https://doi.org/10.1126/science.1157996>.
- (7) Bertolazzi, S.; Brivio, J.; Kis, A. Stretching and Breaking of Ultrathin MoS₂. *ACS Nano* **2011**, *5* (12), 9703–9709. <https://doi.org/10.1021/nn203879f>.
- (8) Qiu, H.; Xu, T.; Wang, Z.; Ren, W.; Nan, H.; Ni, Z.; Chen, Q.; Yuan, S.; Miao, F.; Song, F.; Long, G.; Shi, Y.; Sun, L.; Wang, J.; Wang, X. Hopping Transport through Defect-Induced Localized States in Molybdenum Disulphide. *Nat. Commun.* **2013**, *4* (1), 2642. <https://doi.org/10.1038/ncomms3642>.
- (9) Yang, Y.; Li, X.; Wen, M.; Hacopian, E.; Chen, W.; Gong, Y.; Zhang, J.; Li, B.; Zhou, W.; Ajayan, P. M.; Chen, Q.; Zhu, T.; Lou, J. Brittle Fracture of 2D MoSe₂. *Adv. Mater.* **2017**, *29* (2), 1604201. <https://doi.org/10.1002/adma.201604201>.
- (10) Ly, T. H.; Zhao, J.; Cichocka, M. O.; Li, L.-J.; Lee, Y. H. Dynamical Observations on the Crack Tip Zone and Stress Corrosion of Two-Dimensional MoS₂. *Nat. Commun.* **2017**, *8* (1), 14116. <https://doi.org/10.1038/ncomms14116>.
- (11) Li, M.; Wan, Y.; Wang, W. Prediction of Mechanical Properties for Defective Monolayer MoS₂ with Single Molybdenum Vacancy Defects Using Molecular Dynamics Simulations. In *2017 IEEE 17th International Conference on Nanotechnology (IEEE-NANO)*; 2017; pp 9–12. <https://doi.org/10.1109/NANO.2017.8117324>.
- (12) Hasanian, M.; Mortazavi, B.; Ostadhossein, A.; Rabczuk, T.; van Duin, A. C. T. Hydrogenation and Defect Formation Control the Strength and Ductility of MoS₂ Nanosheets: Reactive Molecular Dynamics Simulation. *Extreme Mech. Lett.* **2018**, *22*, 157–164. <https://doi.org/10.1016/j.eml.2018.05.008>.
- (13) Wang, S.; Qin, Z.; Jung, G. S.; Martin-Martinez, F. J.; Zhang, K.; Buehler, M. J.; Warner, J. H. Atomically Sharp Crack Tips in Monolayer MoS₂ and Their Enhanced Toughness by Vacancy Defects. *ACS Nano* **2016**, *10* (11), 9831–9839. <https://doi.org/10.1021/acsnano.6b05435>.
- (14) Liu, K.; Yan, Q.; Chen, M.; Fan, W.; Sun, Y.; Suh, J.; Fu, D.; Lee, S.; Zhou, J.; Tongay, S.; Ji, J.; Neaton, J. B.; Wu, J. Elastic Properties of Chemical-Vapor-Deposited Monolayer MoS₂, WS₂, and Their Bilayer Heterostructures. *Nano Lett.* **2014**, *14* (9), 5097–5103. <https://doi.org/10.1021/nl501793a>.
- (15) Castellanos-Gomez, A.; Poot, M.; Steele, G. A.; van der Zant, H. S. J.; Agrait, N.; Rubio-Bollinger, G. Mechanical Properties of Freely Suspended Semiconducting Graphene-like Layers Based on MoS₂. *Nanoscale Res. Lett.* **2012**, *7*, 1–4. <https://doi.org/10.1186/1556-276X-7-233>.
- (16) Splendiani, A.; Sun, L.; Zhang, Y.; Li, T.; Kim, J.; Chim, C.-Y.; Galli, G.; Wang, F. Emerging Photoluminescence in Monolayer MoS₂. *Nano Lett.* **2010**, *10* (4), 1271–1275. <https://doi.org/10.1021/nl903868w>.
- (17) Komaragiri, U.; Begley, M. R.; Simmonds, J. G. The Mechanical Response of Freestanding Circular Elastic Films Under Point and Pressure Loads. *J. Appl. Mech.* **2005**, *72* (2), 203–212. <https://doi.org/10.1115/1.1827246>.

- (18) Begley, M. R.; Mackin, T. J. Spherical Indentation of Freestanding Circular Thin Films in the Membrane Regime. *J. Mech. Phys. Solids* **2004**, *52* (9), 2005–2023. <https://doi.org/10.1016/j.jmps.2004.03.002>.
- (19) Parkin, W. M.; Balan, A.; Liang, L.; Das, P. M.; Lamparski, M.; Naylor, C. H.; Rodríguez-Manzo, J. A.; Johnson, A. T. C.; Meunier, V.; Drndić, M. Raman Shifts in Electron-Irradiated Monolayer MoS₂. *ACS Nano* **2016**, *10* (4), 4134–4142. <https://doi.org/10.1021/acsnano.5b07388>.
- (20) Mignuzzi, S.; Pollard, A. J.; Bonini, N.; Brennan, B.; Gilmore, I. S.; Pimenta, M. A.; Richards, D.; Roy, D. Effect of Disorder on Raman Scattering of Single-Layer Mo S₂. *Phys. Rev. B* **2015**, *91* (19), 195411. <https://doi.org/10.1103/PhysRevB.91.195411>.
- (21) Lawn, B. Fracture of Brittle Solids by Brian Lawn /core/books/fracture-of-brittle-solids/B1EC1413BDBA1DCF49E1665D4B0A20F3 (accessed Oct 23, 2019). <https://doi.org/10.1017/CBO9780511623127>.
- (22) Gao, H.; Ji, B.; Jager, I. L.; Arzt, E.; Fratzl, P. Materials Become Insensitive to Flaws at Nanoscale: Lessons from Nature. *Proc. Natl. Acad. Sci.* **2003**, *100* (10), 5597–5600. <https://doi.org/10.1073/pnas.0631609100>.
- (23) Lopez-Polin, G.; Gomez-Herrero, J.; Gomez-Navarro, C. Confining Crack Propagation in Defective Graphene. *Nano Lett.* **2015**, *15* (3), 2050–2054. <https://doi.org/10.1021/nl504936q>.
- (24) Rocha-Rangel, E. Fracture Toughness Determinations by Means of Indentation Fracture. In *Nanocomposites with Unique Properties and Applications in Medicine and Industry*; Cuppoletti, J., Ed.; InTech, 2011. <https://doi.org/10.5772/18127>.
- (25) Bhat, S.; Ukadgaonker, Vijay. G.; Jha, M.; Nirgude, S. M. Fracture Parameter Estimation of Alloy Steel Reinforced with Maraging Steel. In *Fracture of Nano and Engineering Materials and Structures*; Gdoutos, E. E., Ed.; Springer Netherlands: Dordrecht, 2006; pp 359–360. https://doi.org/10.1007/1-4020-4972-2_177.
- (26) Wang, B.; Islam, Z.; Zhang, K.; Wang, K.; Robinson, J.; Haque, A. Role of Sulphur Atoms on Stress Relaxation and Crack Propagation in Monolayer MoS₂. *Nanotechnology* **2017**, *28* (36), 365703. <https://doi.org/10.1088/1361-6528/aa7d9e>.

TOC: Fragility of MoS₂ is overcome via controlled creation of atomic vacancies by ion irradiation. 2D crystals tend to fracture in brittle manner producing catastrophic failure and limiting their reliability. Our systematic study shows that while tears in pristine MoS₂ span microns length, crack propagation is reduced to few nanometers in the presence of controlled induced defects, effectively increasing fracture toughness.

